TURBULENT MIXED CONVECTION HEAT TRANSFER FOR NON-UNIFORM HEAT FLUX DISTRIBUTIONS ON A HORIZONTAL CIRCULAR TUBE

Izuchukwu F. Okafor, Jaco Dirker* and Josua P. Meyer
*Author for correspondence
Department of Mechanical and Aeronautical Engineering,
University of Pretoria, Pretoria, South Africa
*e-mail: jaco.dirker@up.ac.za

ABSTRACT

This study numerically investigated influence of non-uniform circumferential heat flux distributions boundaries on secondary flow, internal heat transfer and friction factor characteristics of a horizontal circular tube in turbulent mixed convection regime. A three dimensional steady-state numerical simulation for inlet Reynolds number of 3 030 to 202 400 was implemented on ANSYS Fluent version 14. The circumferential non-uniform heat flux distribution was simulated as a sinusoidal function of heat flux incident on the tube model. The *k-ε* model was used to simulate the turbulent flow of the heat transfer fluid through the tube model. A steel tube with wall thickness of 5.2 mm, length to inner-diameter ratio of 160 and thermal conductivity of 16.27 W/mK was used. The tube-wall heat conduction and the external heat flux losses via convection and radiation were also considered. It was found that circumferential spans of non-uniform heat flux distributions boundaries have significant effects on the buoyancy-driven secondary flow for Reynolds number range of 3 030 to 9 100. The Richardson number increased with the circumferential span of the heat flux boundary due to buoyancy-effects and the internal heat transfer coefficient was higher than where buoyancy-effect was neglected. Internal heat transfer coefficients and friction factors for non-uniform heat flux cases were found to be higher than the uniform heat flux cases. These revealed that at *Re* less than 9 100, secondary flow effects, heat flux intensities and heat flux distributions boundary type must be considered in determining internal heat transfer and friction factors characteristics of the tube. Internal heat transfer coefficients increased with fluid inlet temperatures, while friction factor decreased with an increase in fluid inlet temperatures. For *Re* above 9 100, internal heat transfer coefficients and friction factors are independent of secondary flow effects, heat flux intensities, circumferential spans of heat flux distributions and heat flux boundary type. This indicates that classical correlations are suitable for higher Reynolds turbulent flow, but in laminar and low Reynolds turbulent flow regimes, classical equations were not suitable for non-uniform heating.

Key words: non-uniform heat flux distributions; turbulent mixed convection; secondary flow; internal heat transfer coefficient; friction factor.

INTRODUCTION

Heat transfer and fluid flow in circular tubes in turbulent regime are very essential in many engineering applications such as heat exchangers, solar thermal collectors, boilers and other industrial equipment. In these systems, the exterior walls of the tubes are usually subjected to either circumferential uniform or non-uniform heat flux boundary conditions. A number of experimental and numerical studies have been conducted for horizontal tubes with uniform heat flux boundary conditions [1-4] for forced-convection flow at high Reynolds numbers and neglecting the low turbulent mixed convection regime. For a horizontal circular tube, under the influence of gravitational field and non-uniform circumferential heating condition, the buoyancy-driven secondary flow in the week turbulent flow regime could still have significant effects on the forced-convection heat transfer and could also differ significantly from that of the uniform

NOMENCLATURE

A	[m^2]	surface or cross sectional area
f	[-]	Darcy friction factor
g	[m/s^2]	acceleration due to gravity
Gr	[-]	Grashof number
$h, \bar{h}$	[W/m^2K]	heat transfer coefficient and average heat transfer coefficient
I	[-]	number of segments which receives heat flux
In	[-]	turbulent intensity
k	[W/m K]	thermal conductivity
L, L_{TOT}	[m]	axial dimension and total axial length of tube
M	[-]	total number of the axial divisions
(m, n)	[-]	numerical surface location
N	[-]	total number of the circumferential divisions
Nu $\overline{\text{Nu}}$	[-]	Nusselt number and average Nusselt number
Pr	[-]	Prandtl number
q	[W]	heat transfer
q''	[W/m^2]	heat flux
R , $\bar{R}$	[m]	radius and average radius
r	[m]	radial coordinate
Re	[-]	Reynolds number
Ri	[-]	Richardson number
$T, \bar{T}$	[K]	temperature and average temperature
t	[m]	tube wall thickness
$v, \bar{v}$	[m/s]	velocity, average velocity
x	[m]	axial coordinate
Greek Letters		
α	[°]	angle span of the heated segment of the tube
β	[K^{-1}]	thermal expansion coef. of heat transfer fluid
θ	[-]	temperature factor
ρ	[kg/m^3]	density of the heat transfer fluid
ϕ	[°]	angle span of each circumferential division or tangential dimension
Subscript		
a , atm		free stream air , atmosphere
∞		radiant surroundings
b		bulk fluid property
conv		convection
f , i		fluid, factor, inner surface
m, n		at position m, n
o		outer surface
r , rad		in radial direction , radiation
tu ,w		tube , wall

heating case. Considering the buoyancy-driven secondary flow phenomenon, the classical heat transfer correlations, for uniform heating condition, could be inappropriate for determining heat transfer characteristics of such a horizontal circular tube with non-uniform heating boundary condition. Studies that could provide information on the effects of buoyancy-induced secondary flow in the weak turbulent mixed convection heat transfer for the non-uniform heat flux boundary cases are still lacking in the literature. This could be due to the complexity of such thermal boundary conditions and the difficulties in achieving the non-uniform thermal boundary conditions in an experimental set-up. Peyghambarzadeh[5] and Grassi and Testi [6] experimentally investigated the turbulent mixed convection in the entrance region for uniformly heated horizontal tubes. The present study numerically investigates the influence of different circumferential spans of non-uniform heat flux distributions boundary on secondary flow, internal heat transfer and friction factor characteristics of a horizontal circular tube in turbulent mixed convection regime. The influence of different fluid inlet temperatures on the internal convective heat transfer coefficient and the friction factors for the tube model in the turbulent mixed convection regime are also investigated for two base-levels non-uniform heat flux intensities.

PHYSICAL MODEL AND PROBLEM DESCRIPTION

Figure 1 gives a representation of the geometry of the tube model being considered in a horizontal orientation. It has an outer radius of R_o = 73 mm, a wall thickness of t = 5.2 mm, length to inner-diameter ratio of approximately 160 and a thermal conductivity of 16.27 W/mK. The tube model is divided into $M \times N$ number of sections in the axial and circumferential directions.

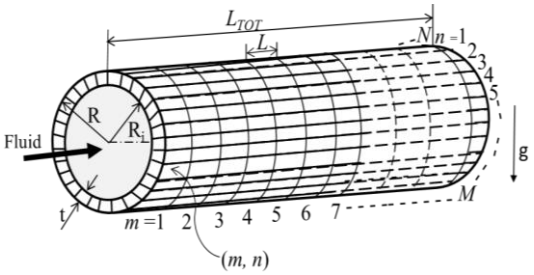

Figure 1 Geometry of the tube model.

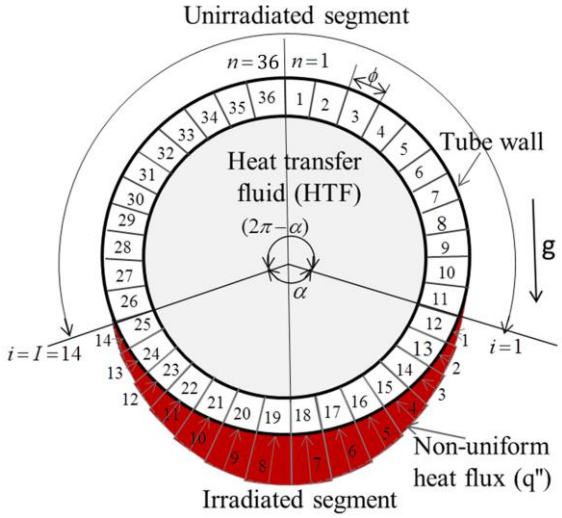

Figure 2 Cross-section of the tube model in Figure 1

Figure 2 is the cross-section of the tube model, under the influence of the gravitational field (g), and non-uniform heat flux distribution flux boundary (indicated by red shading) with maximum intensity from the bottom portion of the tube for a circumferential span of α. The temperature differential along the circumferential wall of the tube due to the non-uniform heat flux distributions could create density variations within the fluid. In the weak turbulent flow regime, the buoyancy-induced secondary flow could have significant effects on the pure forced-convection heat transfer under the non-uniform heating condition and the effects could also differ from that of the uniform heating case. This situation needs to be investigated for the case of a horizontal circular tube. Also, the available heat transfer correlations for uniform heating conditions in the turbulent mixed convection regime may not be suitable for non-uniform heating boundary condition.

NUMERICAL FORMULATION AND HEAT TRANSFER MODEL

In Figure 2, the circumferential wall of the tube model was divided into N = 36 segments for the purpose of simulating the circumferential non-uniform heat flux distributions boundary around the tube. Each of the segments subtends an angle span of ϕ defined as:

$$\phi = \frac{2\pi}{N} \tag{1}$$

The segment, $n_{i=1}$ (in a clockwise fashion) represents where the heat flux distribution starts and can be expressed in terms of N in equation (2).

$$n_{i=1} = \frac{[N-I]}{2} + 1 \tag{2}$$

where $n = 1, 2, 3 \ldots N = 36$, *and* $i = 1, 2, 3 \ldots I$. I is the number of segments of the tube model which directly received the heat flux expressed in equation (3) and α is in the multiple of 20°.

$$I = \frac{\alpha}{2\pi} N \tag{3}$$

By applying the energy balance principle on the element at (n, m) shown in Figure 1, a heat transfer model under steady-state condition can be obtained in equation (4).

$$q_{o,(m,n)} = q_{i,(m,n)} + q_{x,(m,n)} + q_{x,(m+1,n)} + q_{\phi,(m,n)} + q_{\phi,(m,n+1)} + q_{o,conv,(m,n)} + q_{o,rad,(m,n)} \tag{4}$$

Where $q_{o,(m,n)}$ is the heat transfer rate on the outer wall surface at location (m, n) given in equation (5) as follows:

$$q_{o,(m,n)} = q''_{o,(m,n)} A_o \tag{5}$$

$q_{i,(m,n)}$ in equation (4) is the heat transfer rate to the working fluid at location (m, n) expressed as follows:

$$q_{i,(m,n)} = h_{i,(m,n)} . A_{i,(m,n)} (T_{wi,(m,n)} - T_{b,m}) \tag{6}$$

where $h_{i,(m,n)}$ is the local internal heat transfer coefficient, $A_{i,(m,n)}$ is the inner wall surface area, $T_{wi,(m,n)}$ is the inner wall temperature and $T_{b,m}$ is the fluid bulk temperature. The average circumferential internal heat transfer coefficient at

position m, $\bar{h}_{i,m}$, is related to the average Nusselt number at position m as follows:

$$\overline{Nu}_{i,m} = \frac{\bar{h}_{i,m} 2R_i}{k_f} \tag{7}$$

The average circumferential internal heat transfer coefficient can be expressed as:

$$\bar{h}_{i,m} = \frac{\Sigma_{n=1}^{N} q_{i,(m,n)}}{2\pi R_i L\left(\bar{T}_{w,i,m} - T_{b,m}\right)} \tag{8}$$

$\bar{T}_{w,i,m}$ is the circumferential average local inner-wall temperature. $q_{\phi,(m,n)}$ and $q_{\phi,(m,n+1)}$ in equation (4) are the conductive heat transfers in the tangential direction modeled from the Fourier law of heat conduction [7]. Also, $q_{x,(m,n)}$ and $q_{x,(m+1,n)}$ are the conductive heat transfers in the axial direction modeled from Fourier's law of heat conduction. While $q_{o,conv,(m,n)}$ is the forced convective heat transfer loss from the outer-wall surface at (m, n) to the surroundings modeled from Newton's law of cooling and $q_{o,rad,(m,n)}$ is the radiative heat transfer loss to the surroundings modeled from the Stefan-Boltzmann law of emissive [7].

The $\bar{h}_{i,m}$ and $\bar{T}_{w,i,m}$ in equation (8) are determined by performing numerical simulations implemented in ANSYS Fluent version 14.0 [9] for a three dimensional steady-state and turbulent flow at Re = 3 030 to 202 400 for different circumferential spans of uniform and non-uniform heat flux distributions boundaries.

FLUID FLOW THROUGH THE TUBE MODEL

The fluid flow through the tube model in Figure 1 was assumed incompressible, a three dimensional steady-state and turbulent flow. The friction factor (f) for the tube model is expressed in equation (9) in terms of total pressure drop (Δp) over the tube length (L_{TOT}) [8].

$$f = \frac{2R_i}{L_{TOT}} \frac{2}{\rho \bar{v}^2} \Delta P \tag{9}$$

The governing equations for the fluid flow and heat transfer in the tube model were the continuity, momentum and energy equations presented in vector form [10] given as follows:

Continuity: $$\nabla \cdot \vec{V} = 0 \tag{10}$$

Momentum: $$\rho(\vec{V} \cdot \nabla)\vec{V} = -\nabla p + \mu \nabla^2 \vec{V} + \rho \vec{g} \tag{11}$$

Energy: $$V \cdot (\vec{V}(\rho c_p T)) = \nabla \cdot (k \nabla T) \tag{12}$$

where $\nabla \equiv \frac{1}{r}\frac{\partial}{\partial r} + \frac{1}{r}\frac{\partial}{\partial \phi} + \frac{\partial}{\partial x}$ and $\vec{V} = v_r + v_\theta + v_x$

BOUNDARY CONDITIONS

The following boundary conditions were applied:

(i) Inlet boundary conditions (x = 0):

$$\dot{m}_x(r,\phi) = \text{ uniform and } \dot{m}_r = \dot{m}_\phi = 0 \text{ kg/s} \tag{13}$$

$$T_f(r,\phi) = T_{b,o} = 300 \text{ K} \tag{14}$$

(ii) Outlet boundary condition ($x = L_{TOT}$):

$$P(r,\phi) = P_{atmp} \tag{15}$$

The turbulence variables at the inlet and outlet of the tube model were applied using an empirical relation for the turbulence intensity (In) [9] expressed in equation (16):

$$In \equiv \frac{\sqrt{\frac{2}{3}k}}{\bar{v}_{avg}} \cong \frac{0.16}{\text{Re}^{\frac{1}{8}}} \tag{16}$$

(iii) Tube inner wall surface boundary condition (r = R_i):

$$v_r = v_\phi = v_x = 0 \tag{17}$$

(iv) External wall surface boundary conditions ($r = R_o$):

The external wall surface boundary conditions used for the uniform and non-uniform heat flux distributions are given in Table 1. Two different heat flux intensities base-levels, q'' =7.1 kW/m^2 and 14.7 kW/m^2 were used. The sinusoidal function in Table 1 was based on the ray-tracing of heat flux distribution simulation results of Häberle *et al*. [11], where the lower segments of the tube model received the higher heat transfer rates and then decreased towards the upper segments, as in the case of the absorber tube receiver of a linear Fresnel solar collector.

(v) Near-wall flow boundary condition:

The k-ε two-equation turbulence model cannot be applied in the regions close to the solid boundary where viscous effects are dominant over turbulence [12]. The standard wall function in ANSYS Fluent [9] was adopted for solving the near-wall region flow in the tube inner-wall.

Table 1 External surface heat transfer boundary conditions

Heat flux distribution	**Heat transfer on external surface**	**Wall element range**
1) Irradiated Elements: (i) Sinusoidal non-uniform heat flux cases:	$q''_{o,(m,n)} = q'' \times \sin \times \left[\frac{\pi}{\alpha}\phi(n - n_{i=1} + \frac{1}{2})\right]$	$m \in [1, M]$ and $n \in [n_{i=1}, n_{i=1} + I)$
(ii) Uniform heat flux cases:	$q''_{o,(m,n)} = q'' \frac{2}{\pi}$	$m \in [1, M]$ and $n \in [n_{i=1}, n_{i=1} + I)$
2) Unirradiated element:	$q''_{o,(m,n)} = 0$	$m \in [1, M]$ and $n \notin [n_{i=1}, n_{i=1} + I)$
Associated fully uniform heat flux cases:	$q''_{o,(m.n)} = q'' \frac{\alpha}{\pi^2}$	$m \in [1, M]$ and $n \in [n_{i=1}, n_{i=1} + I)$

NUMERICAL METHOD AND MODEL VALIDATION

Equations (10) – (12) were solved numerically by the finite volume method described by Patankar [13]. The convective terms in the momentum and energy equations were discretised and solved using a second-order upwind scheme and the standard SIMPLEC algorithm was used for the pressure-velocity coupling. The k-ε model was used to simulate the turbulent flow of the heat transfer fluid through the tube model and standard wall function was used for solving the near-wall region flow problems. A series of grid independence study was conducted in terms of the outlet temperature rise of the heat transfer fluid to ensure that the grid was sufficiently fine not to have a significant impact on the numerical results. The convergence criteria for the continuity, momentum and energy equations were set at minimum residual values of 10^{-6} and 10^{-8} respectively. The heat flux boundary conditions in Table 1 were implemented according to the angular position of the boundary cell via user defined functions. The thermal properties of the heat transfer fluid and the tube material were assumed constant

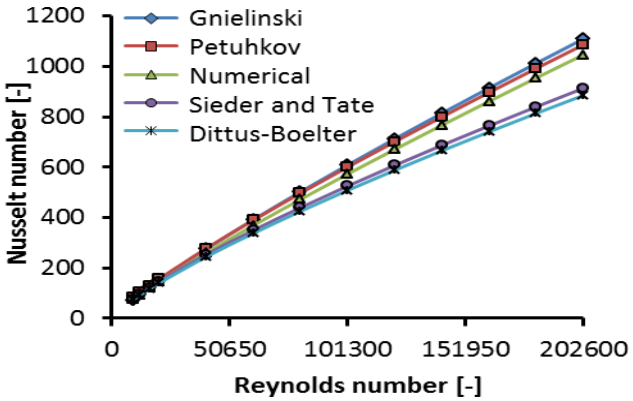

Figure 3 Numerical Nusselt number compared with Nusselt number experimental correlations.

and independent of temperature, except for the fluid density (ρ) [8] expressed as temperature dependent [$\rho = \rho_o(1\text{-}\beta\Delta T)$].

The model was validated by comparing the numerical friction factor and Nusselt number values with friction factor and Nusselt number correlations [8] in terms of *f*, *Re*, and *Pr*, for turbulent flow in circular tubes, for uniform heat flux base-level intensity of 7.1 kW/m^2. Figure 3 shows that the numerical results agreed with the Nusselt number correlations and that of the friction factor (figure not shown here).

RESULTS AND DISCUSSION

Figure 4 is the visual results indicating the temperature contours for different circumferential span (α) of the sinusoidal non-uniform heat flux distributions base-level intensity of 7.1 kW/m^2, in the low turbulent flow regime and Reynolds number of 5 100.

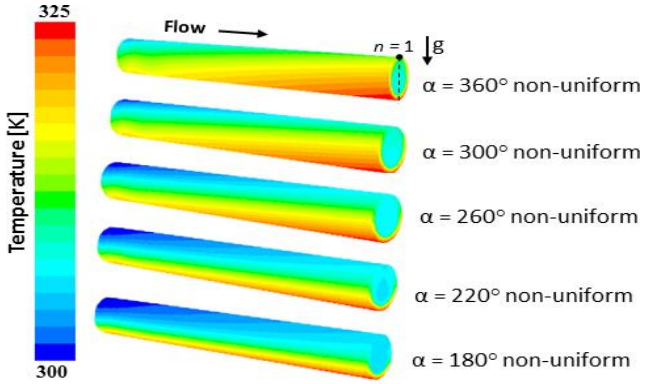

Figure 4 Temperature contours for different circumferential sinusoidal non-uniform heat flux distributions.

The non-uniformity of the tube-wall temperature in Figure 4 is demonstrated in Figure 5, where the non-uniform temperature factor, θ_f defined in equation (18) is plotted against the circumferential position (n) for different α values.

$$\theta_f = \frac{T_{w,o,(n)} - T_b}{\overline{T}_{w,i,(n)} - T_b} \tag{18}$$

$$\overline{T}_{w,i,n} = \frac{1}{N}\sum_{n=1}^{N} T_{w,i,(m,n)}$$

$\overline{T}_{w,i,(n)}$ is the local average circumferential inner-wall temperature and $T_{w,o,(n)}$ is the local outer-wall temperature of the tube for segment *n*.

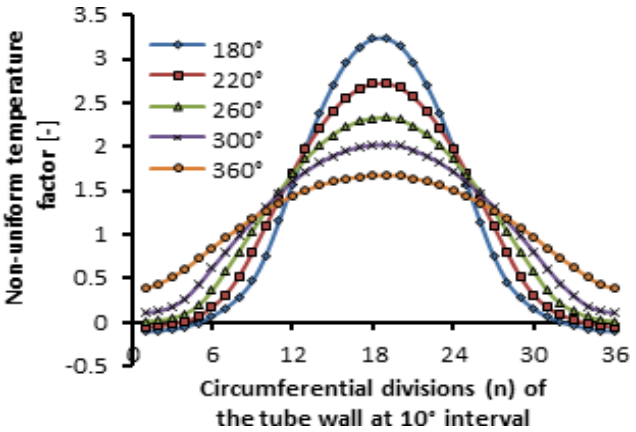

Figure 5 Non-uniform temperature factors at different spans of non-uniform heat flux distributions boundaries.

Figure 10 shows that θ_f is maximum at the peak of the profiles (n ≈ 18 and 19), which corresponds to the lower central portion of the tube with the maximum incident heat flux. In equation (18), for $\theta_f = 0$, the outer-wall temperature is equal to the bulk fluid temperature, which implies no heat transfer from the outer-wall to the fluid at segment *n*. For $\theta_f > 0$, it indicates significant heat transfer from the outer-wall to the fluid at segment *n*. Towards the two ends of the profiles, $\theta_f < 0$ indicating heat loss from the fluid at segment *n* and this occurred towards upper region of the tube which received insignificant heat flux.

Richardson number for non-uniform heat flux heat flux boundaries

For a horizontal tube with a circumferential non-uniform heating, a secondary flow motion is induced due to fluid density differential. This result in counter-rotating transverse vortices superimposed on the axial pure forced-convection flow, which increases the fluid mixing and thereby increasing the internal heat transfer rate. The Richardson number (*Ri*) [8] expressed in equation (19) indicates the relative strength of the induced buoyancy-driven secondary flow to the pure forced-convection flow in the tube.

$$Ri = \frac{Gr}{\mathrm{Re}^2} = \frac{g\beta(2R_i)^3\Delta T V^{-2}}{2R_i\rho\nu/\mu} \tag{19}$$

Re is the Reynolds number and *Gr* is the Grashof number.

Figure 6 shows that *Ri* increased with an increase in the circumferential span of the non-uniform heat flux boundary on the horizontal tube and the increase was more pronounced at the lower turbulent Reynolds number. This indicates that the buoyancy-induced secondary flow due to the non-uniform on heat flux distributions boundary has significant effects in the turbulent mixed convection regime. Also, *Ri* decreased with an increase in Reynolds number, which shows a stronger buoyancy effects at lower Reynolds numbers and a weaker buoyancy effects at higher Reynolds numbers. It can be seen in Figure 6 that at *Re* = 5 100, 6 100 and 7 100 for α = 140° to 360° and *Re* = 9 100 for α = 220° to 360° are all in the range of 0.1< *Ri* < 10, which indicated that the turbulent mixed convection heat transfer dominated in this Reynolds number range. For *Re* = 16 200, *Ri* < 0.1 for all the spans of the heat flux distributions boundaries considered, indicating that buoyancy effect was negligible and that forced-convection dominated the heat transfer processes.

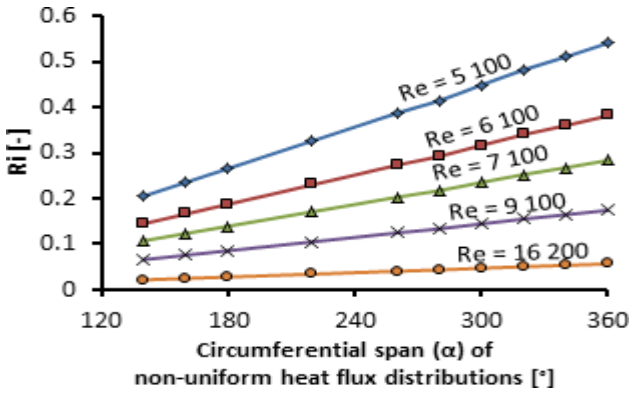

Figure 6 *Ri* for sinusoidal non-uniform heat flux distribution base-level intensity of 7.1 kW/m^2 at different *Re*.

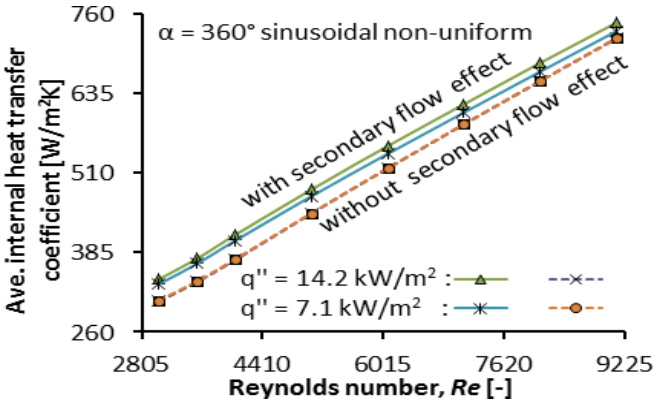

Figure 7 Variation of internal heat transfer coefficients with *Re* for different base-levels heat flux intensities, with and without secondary flow effect.

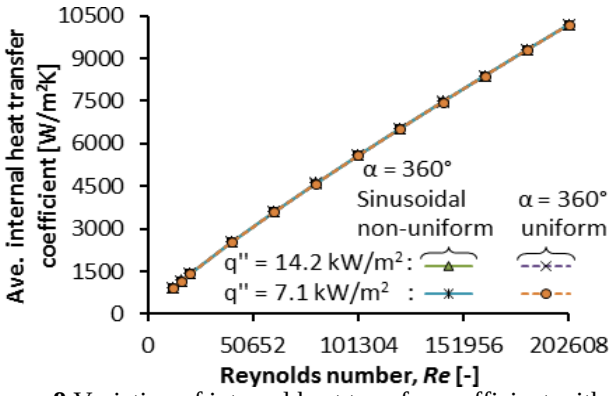

Figure 8 Variation of internal heat transfer coefficient with *Re* for different base-levels heat flux intensities, where secondary flow effect was neglected.

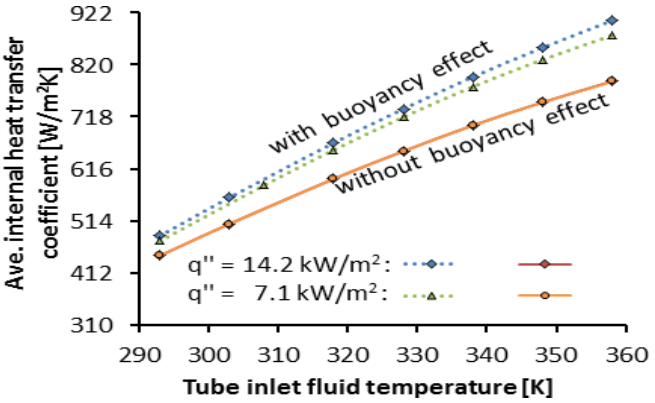

Figure 9 Ave. internal heat transfer coefficients at different inlet fluid temperatures for α = 320° span of non-uniform heat flux distribution, with and without buoyancy effect at inlet *Re* = 5 050 to 15 100.

Heat transfer coefficients for uniform and non-uniform heat flux boundaries

The impact of buoyancy-induced secondary flow on pure forced-convection heat transfer in the weak turbulent flow regime is demonstrated in Figures 7, 8 and 9. For inlet Re = 3 030 to 9 100 in Figure 7, where buoyancy effect was neglected, represented with dotted lines, there was no significant difference in the internal heat transfer coefficients for the base-levels heat flux intensities. The internal heat transfer coefficients for the base-level heat flux intensities of 14.2 kW/m^2 and 7.1 kW/m^2 were up to 13 % and 10 % higher than where buoyancy effect was neglected. This indicates that influence of buoyancy-driven secondary flow cannot be neglected for *Re* less than 9 100. Otherwise, the internal heat transfer coefficients would be under-estimated. Figure 8 indicates that for inlet *Re* = 12 100 to 202 400, internal heat transfer coefficients are independent of secondary flow effects, heat flux intensities and heat flux distributions boundary type. This could be due to a very weak influence of buoyancy-driven secondary flow at higher turbulent flow regime. This revealed that for *Re* = 12 100 and above, the classical heat transfer correlations could be used without modification to account for non-uniform tube-wall temperature variations.

In Figure 9, where buoyancy effect was present, the internal heat transfer coefficient values were up to 15 % higher than where it was neglected. This revealed that the buoyancy effects due to the circumferential non-uniform heat flux distributions boundary for a horizontal circular tube must be considered in determining the internal heat transfer in the turbulent flow regime for *Re* less than 9 100. Also, the internal heat transfer coefficient increased up to 76% by increasing the fluid inlet temperature from 293 K to 360 K, at the same ambient temperature. This indicates the influence of pre-heating the inlet heat transfer fluid on the internal heat transfer coefficient of a horizontal circular tube.

Friction factors for uniform and non-uniform heat flux heat flux boundaries

In Figure 10, at *Re* = 3 030, the friction factor values for non-uniform and uniform heat flux cases were 21 % and 16% higher than the pure forced-convection and decreased to less than 1% at Re = 9 100. This revealed that the buoyancy-induced secondary flow is still significant at low turbulent flow regime and decreased as *Re* increased. It also differed for different types of heat flux distributions boundaries. In Figure 11, sinusoidal non-uniform case represented with solid lines differentiated the non-uniform heating from the usual assumption of uniform heating for a horizontal tube heated from below. It indicates that circumferential span of heat flux distributions boundary has a significant effect on buoyancy-driven secondary flow, especially at higher angle span. Thus, friction factor values and heat transfer rates would be under-estimated if uniform heat flux was assumed where the actual heat flux distribution boundary was non-uniform.

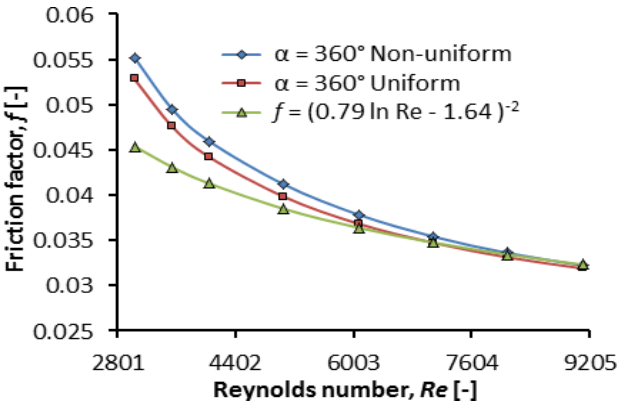

Figure 10 Variation of friction factors with *Re*

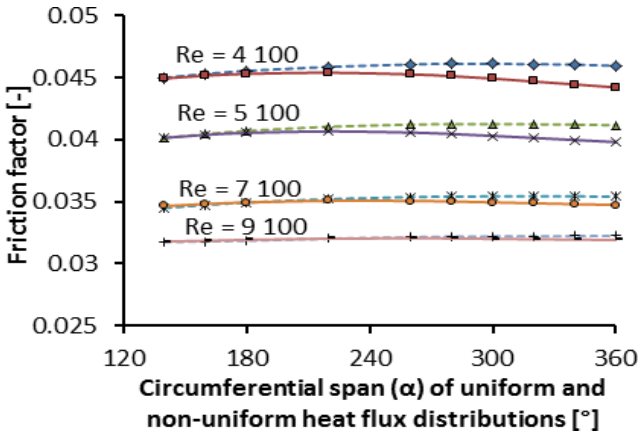

Figure 11 Variation of friction factors with *Re* for uniform and sinusoidal non-uniform heat flux base-level intensity of 7.1 kW/m^2 at the inlet *Re* = 4 100 and 9 100.

In Figure 12, where buoyancy effect was present, the friction factor values were up to 16 %, higher than where it was neglected. This revealed that the buoyancy effect due to the circumferential non-uniform heat flux distribution boundary for a horizontal circular tube must be considered in determining the friction factor characteristics in the turbulent flow regime for *Re* less than 9 100. Also, the friction factor decreased up to 22% by increasing the fluid inlet temperature from 293 K to 360 K, at the same ambient temperature. This indicates the influence of pre-heating the inlet heat transfer fluid on the friction factor of a circular tube.

CONCLUSION

The numerical results indicated that buoyancy-driven secondary flow must be considered in determining the internal heat transfer and friction factor characteristics of a horizontal circular tube at weak turbulent flow regime. The classical heat transfer correlations for uniform heating conditions would be inappropriate for non-uniform heating cases for *Re* less than 9 100. Also, the internal heat transfer coefficients increased with the fluid inlet temperatures, while friction factor decreased with an increase in fluid inlet temperatures. However, for *Re* higher than 9 100, internal heat transfer coefficients and friction factors are independent of secondary flow effects, heat flux intensities and heat flux distributions boundary type. This indicates that the classical heat transfer correlations could be used without modifications to account for the tube-wall temperatures variations due to non-uniform heat flux boundary.

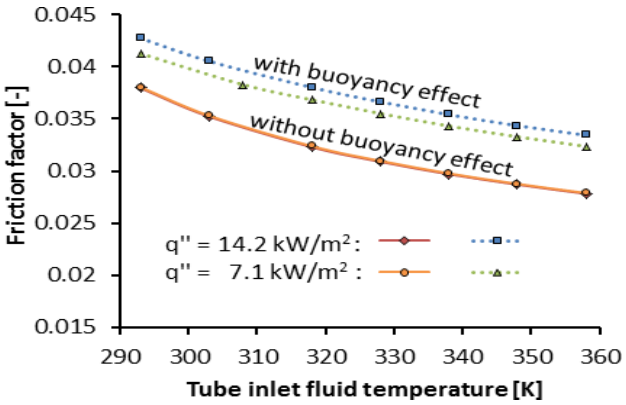

Figure 12 Friction factors at different inlet fluid temperatures for α = 320° sinusoidal non-uniform heat flux base-level intensities of 14.2 kW/m^2 and 7.1 kW/m^2, with and without buoyancy effect at inlet *Re* = 5 050 to 15 100.

ACKNOWLEDGEMENT

The funding received from DTI/NRF, CSIR and University of Pretoria is duly acknowledged.

REFERENCES

[1] Mori Y., Futagami K., Tokuda S.and Nakamura M., Forced Convective Heat Transfer in Uniformly Heated Horizontal Tubes 1st Report-Experimental Study on the Effect of Buoyancy, Inter. Journal of Heat and Mass Transfer 9(5) pp. 453-463, (1966).

[2] Ghajar A. J. and Tam L.-M., Flow Regime Map for a Horizontal Pipe with Uniform Wall Heat Flux and Three Inlet Configurations, Exp. Thermal and Fluid Sc.10 pp. 287-297 (1995).

[3] Hasegawa S. and Fujita Y., Turbulent Heat Transfer in a Tube with Prescribed Heat Flux, Int. J. Heat Mass Transfer 11(1968) 943 – 962.

[4] Elshafei E. A. M., Mohamed M. S., Mansour H. and Sak M. Numerical study of heat transfer in pulsating turbulent air flow Journal of Engr. and Technology Research 4(5), (2012) 89-97.

[5] Peyghambarzadeh S. M., Forced Convection Heat Transfer in the Entrance Region of Horizontal Tube under Constant Heat Flux, World Applied Sciences Journal 15 (3) pp. 331-338 (2011).

[6]Grassi W. and Testi D., Heat Transfer Correlations for Turbulent Mixed Convection in the Entrance Region of a Uniformly Heated Horizontal Tube, J. of Heat Transfer, 128 (2006)1103 -1107.

[7] Rajput R. K., 2005. Heat and Mass Transfer in SI Units. Second Edition. Published by S. Chand and Company Ltd, Ram Nagar, New Delhi, 110 055.

[8] Cengel Y. A, Heat and Mass Transfer: A Practical Approach, Third Edition. Published by McGraw-Hill Companies, Inc. 1221 Avenue of the Americas, New York, NY 10020, (2007).

[9] ANSYS Fluent version 14.0, Users' Guide ANSYS, Release 14.0 Incorporated, Southpointe 275 Technology Drive Canonsburg, PA 15317 (2011).

[10] Vikram R., Snehamoy M. and Dipankar S., Analysis of the Turbulent Fluid Flow in an Axi-symmetric Sudden Expansion. International Journal of Engineering Science and Technology. 2(6) pp. 1569-1574, (2010).

[11] Häberle A, Zahler C., Lerchenmüller H., Mertins M., Wittwer C, Trieb F.and Dersch J., The Solarmundo Line Focusing Fresnel Collector: Optical and Thermal Performance and Cost Calculations, Solarpaces-CSP Technology ISE pp. 1-11, (2002).

[12] Nurnberg P. G., An Exp. and Numerical Investigation of Mixed Convection in Rectangular Enclosures, Open Access Dissertations and Theses, Paper 3956 (1994).

[13] Patankar S.V., Numerical Heat Transfer and Fluid Flow, Hemisphere Publishing Corporation, USA America, (1980).